

Chapter 7

Design Considerations

The details of the specific features of the heat transfer coefficient, and pressure drop estimation have been covered throughout the previous chapters. The objective of this chapter is to summarize important theoretical solutions, results of numerical calculations and experimental correlations that are common in micro-channel devices. These results are assessed from the practical point of view so that they provide a sound basis and guidelines for the evaluation of heat transfer and pressure drop characteristics of single-phase gas–liquid and steam–liquid flows.

7.1 Single-Phase Flow

Fully developed flows in smooth channels

The Poiseuille number in laminar flows is constant but dependent upon the flow passage geometry (Shah and London 1978). The heat transfer rate in laminar channel flow is very sensitive to the thermal boundary conditions. Hence, it is essential to carefully identify the thermal boundary conditions in laminar flow. A systematic analysis of thermal boundary conditions for internal flow is given by Shah and London (1978). Three important thermal boundary conditions T, H1, and H2 are described; they are pertinent to most micro-devices. The T boundary condition refers to the constant wall temperature T_w both axially and peripherally throughout the passage length. The wall heat transfer rate is constant in the axial direction while the wall temperature at any cross-section is constant in the peripheral direction for the H1 boundary condition. The wall heat transfer rate is constant in the axial direction, as well as in the peripheral direction for the H2 boundary condition. The H1 boundary condition is realized at $q_w = \text{const.}$ for highly conductive materials for which the temperature gradients in the peripheral direction are minimum; the H2 boundary condition is realized at $q_w = \text{const.}$ for very low conductive materials for which temperature gradients exist in the peripheral direction. For intermediate values of thermal conductivity, the boundary condition at $q_w = \text{const.}$ will be between H1 and

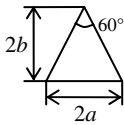
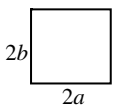
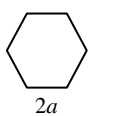
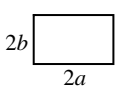
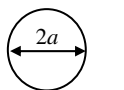
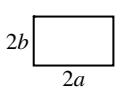
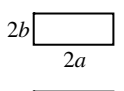
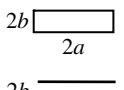
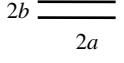
H2. It may be noted that the H1 and H2 boundary conditions for the symmetrically heated passages with no sharp corners (e.g., circular, flat, and concentric annular channels) are identical; they are simply designated as H.

The values of the Nusselt and the Poiseuille numbers for heat transfer and friction for fully developed laminar flows through specified channels are presented in Table 7.1 (Shah and London 1978).

Correlations concerning symmetrically heated channels should be adjusted for non-uniform circumferential heating. An example is given in Sect. 6.4.2, Eqs. (6.53), (6.54), and (6.55).

Theoretical solutions have been verified by many researchers for flow friction and heat transfer in a single channel. Hence, these results provide a valuable guideline for devices that may employ many such channels in parallel. However, passage-

Table 7.1 The Nusselt and the Poiseuille numbers for fully developed laminar flow

Geometry ($L/d_h > 100$)	Nu_{H1}	Nu_{H2}	Nu_T	Po
 $\frac{2b}{2a} = \frac{\sqrt{3}}{2}$	3.111	1.892	2.47	53.332
 $\frac{2b}{2a} = 1$	3.608	3.091	2.976	56.908
	4.002	3.862	3.34	60.216
 $\frac{2b}{2a} = \frac{1}{2}$	4.123	3.017	3.391	62.192
	4.364	4.364	3.657	64
 $\frac{2b}{2a} = \frac{1}{4}$	5.331	2.94	4.439	72.932
 $\frac{2b}{2a} = \frac{1}{4}$	6.049	2.93	5.137	78.808
 $\frac{2b}{2a} = \frac{1}{8}$	6.490	2.94	5.597	82.340
 $\frac{2b}{2a} \rightarrow 0$	8.235	8.235	7.541	96.00

to-passage flow non-uniformity could result in significant deviations in Nu and Po from the analytical predictions. Also, actual thermal boundary conditions for heat transfer may not correspond to any previously described boundary conditions. In addition, the developing flow effect may be present if the flow passage is not long enough. These and other effects such as fouling, fluid property variations, etc., could affect the actual Nu and Po as presented in Table 7.1. For all these reasons, when accurate Nu and Po are needed for specific applications, they should be obtained experimentally or from numerical calculations even for simple passage geometries.

For smooth micro-channels the transition from laminar to turbulent flow occurs at $Re = 1,500-2,200$. For turbulent flows the friction factor maybe calculated as

$$\lambda = 0.316 \cdot Re^{0.25} . \quad (7.1)$$

Direct measurements of turbulent heat transfer in smooth pipes led to the correlation known as the Dittus–Boelter equation

$$Nu = 0.023 \cdot Re^{0.8} Pr^n \quad (7.2)$$

where n is 0.4 and 0.3 for heating and cooling, respectively, Re is the Reynolds number, and Pr is the Prandtl number. The analytical solutions, e.g., Eq. (6.36), based on the thermal boundary approach appears to provide a reasonable basis for understanding the mechanism of heat transfer.

Entrance effects

For most channels, the mean Nusselt number and friction factor will be within 10% of the fully developed value if $L/d_h > 0.2RePr$. If $L/d_h < 0.2RePr$, the fully developed analytical solutions may not be adequate, since Nu and λ are higher in the developing flow region. However, if the passage-to-passage non-uniformity exists in a micro-device, it reduces Nu substantially, and also reduces λ slightly (and it could be neglected for practical purposes).

Effect of roughness

For channels above $d_h = 1$ mm the surface roughness generally does not affect Nu and λ as long as the height of the surface roughness is negligible compared to the channel hydraulic diameter (i.e., $k_s/d_h < 0.01$). For small diameter tubes ($d_h < 0.6$ mm) the relative roughness of $k_s/d_h > 0.003$ increases heat transfer up to 25–30% in the range of $Re = 1,000-2,200$. This effect is more pronounced at higher values of k_s/d_h and Re (Kandlikar et al. 2003).

Axial conduction in the walls

For high values of the Reynolds number, the mean value of the Nusselt number does not differ significantly from the theoretical value for fully developed flow. On the contrary, at low Re the effects of conjugate heat transfer on the mean value of

the Nusselt number are very important because conduction along the channel walls becomes a competitive mechanism to heat transfer through internal convection.

The mean heat transfer coefficient calculated using average wall and fluid temperatures (assuming a linear wall and fluid temperature distribution) is not consistent with mechanisms of heat transfer. This is also an explanation for the dependence of the Nu on Re found in experiments. This effect will decrease as the convective term of heat transfer increases with respect to the conductive term in the channel wall (Hetsroni et al. 2004; Tiselj et al. 2004; Maranzana et al. 2004). This is evidenced through numerical simulation, and when the effects of conjugate heat transfer dominate, the temperature distribution along the micro-channel is not linear. For a circular tube, the region of significance of axial conduction in the walls in the conjugated heat transfer problem, used also by Celata et al. (2005) may be calculated as:

$$(k_w/k_L) ((d_o^2 - d_{in}^2)/d_{in}L) / \text{RePr} > 10^{-2} \quad (7.3)$$

where k_w and k_L is the thermal conductivity of wall and liquid, respectively, d_o and d_{in} is the outer and inner tube diameter, and L is the tube length.

The dimensionless quantity on the left-hand side of Eq. (7.3) labeled as M by the above-cited authors, allows for the comparison of heat transfer by axial conduction in the wall to the convective heat transfer in the flow.

7.2 Gas–Liquid Flow

Void fraction

The void fraction data was obtained in micro-channels and showed significant differences from conventional size channels, depending on the channel cross-section and inlet geometry. For the micro-channels with a diameter of 100 μm , the effects of inlet geometry and the gas–liquid mixing method on the void fraction were seen to be quite strong, while the conventional size channels have shown a much smaller effect of inlet geometry on the void fraction. The homogeneous flow model and the Armand (1946) correlation, $\alpha = \beta$, where $\beta = U_{GS}/(U_{GS} + U_{LS})$, or the correlation $\alpha = 0.83\beta$ recommended by Ali et al. (1993) may be used for narrow channels with $d_h \sim 1 \text{ mm}$.

Kawahara et al. (2002) presented void fraction data obtained in a 100 μm micro-channel connected to a reducing inlet section and T-junction section. The superficial velocities are $U_{GS} = 0.1\text{--}60 \text{ m/s}$ for gas, and $U_{LS} = 0.02\text{--}4 \text{ m/s}$ for liquid. The void fraction data obtained with a T-junction inlet showed a linear relationship between the void fraction and volumetric quality, in agreement with the homogeneous model predictions. On the contrary, the void fraction data from the reducing section inlet experiments showed a non-linear void fraction-to-volumetric quality relationship:

$$\alpha = 0.03\beta^{0.5}/(1 - 0.97\beta^{0.5}). \quad (7.4)$$

Pressure drop

This matter was discussed in Sect. 5.8. For channels of $d_h = 0.9\text{--}3.2$ mm, the two-phase pressure drop can be calculated using the Lockhart–Martinelli model with parameter C , ranging from 5 to 20. The parameter C decreases when the hydraulic diameter decreases (Zhao and Bi 2001). For channels of $d_h = 100\ \mu\text{m}$, (Kawahara et al. 2002) two-phase pressure drop can be correlated within an accuracy of $\pm 10\%$ using the Lockhart–Martinelli model with $C = 0.24$.

Heat transfer

There is a lack of information on the effect of superficial liquid and gas velocities on heat transfer in micro-channels. We studied this problem in the test section that contained 21 parallel triangular micro-channels of $d_h = 130\ \mu\text{m}$.

The heat transfer coefficient h increases with increasing superficial liquid velocity U_{LS} . Enhancement of heat transfer is more pronounced for low values of superficial liquid velocity. An increase in superficial gas velocity U_{GS} to the same value of the superficial liquid velocity led to a decrease in the heat transfer coefficient. The Nusselt number may be calculated as:

$$\text{Nu}_L = 0.044\text{Re}_{LS}^{0.96}\text{Re}_{GS}^{-0.18} \quad \text{for} \quad \text{Re}_{GS} = 4.7\text{--}270, \quad \text{Re}_{LS} = 4.0\text{--}8.0 \quad (7.5)$$

$$\text{Nu}_L = 0.13\text{Re}_{LS}^{0.96}\text{Re}_{GS}^{-0.40} \quad \text{for} \quad \text{Re}_{GS} = 4.7\text{--}270, \quad \text{Re}_{LS} = 8.0\text{--}56 \quad (7.6)$$

where $\text{Nu}_L = hd_h/k_L$, $\text{Re}_{LS} = U_{LS}d_h/\nu_L$, $\text{Re}_{GS} = U_{GS}d_h/\nu_G$, h is the heat transfer coefficient, k_L is the liquid thermal conductivity, U_{LS} and U_{GS} are the liquid and gas superficial velocities, respectively, and ν_L and ν_G are the liquid and gas kinematic viscosity, respectively.

7.3 Boiling in Micro-Channels

7.3.1 Boiling Incipience

Wall superheat

Experimental and analytical studies showed that wall superheat significantly depends on the heat flux. This dependence is close to $\Delta T_{S,ONB} \sim q_{ONB}^{0.5}$. Wall superheat corresponding to nucleate boiling may be calculated using Eq. (6.9).

Effect of pressure

Empirical correlation (6.14) by Bergles and Rohsenow (1964) is recommended when taking the dependence of wall superheat on pressure into account. It agrees fairly well with the prediction of theoretical analysis based on the Hsu (1962) model.

Liquid subcooling at ONB point

For qualitative analysis of the conditions at which the ONB phenomenon takes place the parameter $D = \Delta T_{\text{sub,ONB}}/T_S$ may be used. Depending on the value of D , the channels can be subdivided into two groups: (1) $D < 1$ (parameter is in the range of $D = 0.1-0.5$), and (2) $D \ll 1$ (parameter is in the range of $D = 0.01-0.1$). For the first group, defined as “short channels,” the relative heated length is $L_{\text{ONB}}/d_h < 100$. For the second group, defined as “long channels,” the relative heated length is $L_{\text{ONB}}/d_h > 100$. When the value of D lies in the range of 0.125–0.25, as in experiments by Bergles and Rohsenow (1964), the onset of nucleate boiling occurred at values of the bulk temperature $T_{B,\text{ONB}}$, significantly less than the saturation temperature. When the parameter was in the range of $D = 0.011-0.074$, as in the experiments by Celata et al. (1997) and by Kennedy et al. (2000), the ONB occurred at values of the bulk temperature that were close to saturation. Equations (6.32), (6.33) and (6.34) are suggested for calculation of L_{ONB} at given values of q_{ONB} , inlet velocity, and the difference between saturated and inlet temperature.

Effect of mass flux

Heat flux q_{ONB} is essentially independent of mass flux in the case that the inlet fluid temperature does not differ significantly from the saturation temperature, i.e., $T_S - T_{\text{in}}$ is about 10–20 K. Heat flux q_{ONB} is in excess of 10–20% for the case of $T_S - T_{\text{in}} > 20$ K.

Effect of inlet temperature

Incipient boiling heat flux q_{ONB} decreases with an increase in the inlet temperature. It was shown in Sect. 6.1.4 that an increase in the inlet flow temperature may lead to a drastic decrease in q_{ONB} . As a consequence of the above discussion the fact is that at the same value of T_{in} the value of q_{ONB} increases with increasing inlet velocity (see Eqs. 6.32, 6.33, and 6.34).

Boiling incipience in surfactant solutions

Under some conditions boiling incipience in surfactant solutions may be quite different from that in Newtonian fluids. For some kinds of degraded solutions (i.e., solutions that were used after 6–10 runs) boiling occurred at wall superheat higher than that observed in fresh solutions or water. Hysteresis was observed during boiling of degraded solutions. It is speculated that molecules of degraded surfactant are more amenable to the formation of a surfactant monolayer, which renders the interface less flexible and results in the dampening of interfacial motion.

Effect of dissolved gases

Desorption of the dissolved bubbles formed bubbles of gas and a limited amount of bubbles containing gas–water vapor mixture. As a result, boiling incipience oc-

curs at a channel wall temperature below that of the saturation temperature. Onset of nucleate boiling in surfactant solutions that contain dissolved gases takes place at surface temperatures significantly higher than the saturation temperature (Klein et al. 2005).

Dynamics of vapor bubble

In micro-channels the maximum length of the bubble in the streamwise direction is about eight times larger than that in the spanwise direction (Hetsroni et al. 2003b). The parameter $\Pi = q/(\rho_L U c_{pL} \Delta T_s)$ may be used to distinguish linear and exponential regimes of bubble growth. Bubble formation causes pressure and temperature fluctuations.

7.3.2 Flow Boiling: Pressure Drop Characteristics

Predictions of the homogeneous equilibrium flow model and previous separated flow models yielded relatively poor predictions of pressure drop. The mean absolute error (Eq. 6.48) is in the range of $MAE = \pm 40\%$ (Qu and Mudawar 2003a). A new approach was developed to improve the accuracy of pressure drop prediction in two-phase micro-channels (Lee and Mudawar 2005a). Since the bubbly and churn flow patterns are rarely detected in high-flux micro-channel flow, the separated flow model was deemed more appropriate than the homogeneous. In both the slug and annular regimes, mass transfer by liquid break-up and deposition is highly influenced by surface tension. It is assumed that the added complexity of two-phase flow in a micro-channel is the net result of interactions between liquid inertia, the liquid viscous force, and surface tension. Two key measures of these interactions are the Reynolds number (Eq. 6.47) and Weber number (Eq. 6.48) based on liquid properties. Equations (6.50), (6.51), and (6.52) are suggested to evaluate the pressure drop in a copper micro-channel heat sink. These correlations were examined experimentally by measurements of the pressure drop in water and refrigerant R-134a in a two-phase micro-channel heat sink containing parallel $231 \times 713 \mu\text{m}$ channels. The operating conditions for water were as follows: inlet temperature of $T_{in} = 30.0$ or 60.0°C , mass flux of $G = 135\text{--}400 \text{ kg/m}^2\text{s}$, heat flux of $q = 40.0\text{--}130 \text{ W/cm}^2$, and outlet pressure of $P = 2$ bar. Experiments performed with refrigerant R-134a spanned the following conditions: inlet pressure of $P_{in} = 1.44\text{--}6.60$ bar, mass flux of $G = 127\text{--}654 \text{ kg/m}^2\text{s}$, inlet quality of $x_{in} = 0.001\text{--}0.25$, outlet quality of $x_{in} = 0.001\text{--}0.25$, and heat flux of $q = 31.6\text{--}93.8 \text{ W/cm}^2$. Equations (6.50), (6.51), and (6.52) predict the pressure drop with the mean absolute error of $MAE = \pm 30\%$. New experiments should be performed in micro-channels of different geometry and a comprehensive method should be developed for determining micro-channel heat sink pressure drop for coolants with different thermophysical properties.

7.3.3 Flow Boiling: Heat Transfer

The correlations considered below may be used only in the range of experimental conditions at which these correlations were obtained. More local data for different channel geometries should be obtained for further validating its applicability to different flow regimes, aspect ratios, sizes and geometries.

Nucleate boiling and annular film evaporation

The study by Steinke and Kandlikar (2004) was performed for water flow boiling in six parallel, horizontal, lightly trapezoidal micro-channels of $d_h = 207 \mu\text{m}$. The ranges of parameters are: mass flux from 157 to 1,782 $\text{kg}/\text{m}^2 \text{s}$, heat flux from 5 to 930 kW/m^2 , inlet temperature of 22 °C, quality from sub-cooled to 1.0, and atmospheric pressure at the exit. Equations (6.57), (6.58) and (6.59) were suggested to calculate the heat transfer coefficient. The optimal range of the correlations is between qualities of 0.2 to 0.8. The correlation underpredicts the heat transfer coefficients at the ONB condition. In a recent publication, Kandlikar (2004) presented two new non-dimensional groups that are thought to be important in micro-channel flows. The groups are based on the surface tension and momentum change due to evaporation, as well as the viscous shear force and inertia force. This and prior studies by other authors pointed to annular flow as the dominant two-phase flow pattern in micro-channels at moderate to high heat fluxes. These observations lend credence to the hypothesis that the dominant heat transfer mechanism for two-phase heat sinks is forced convective boiling and not nucleate boiling. It should be stressed that the empirical correlations (6.57), (6.58) and (6.59) predict a heat transfer coefficient about twice that measured by Qu and Mudawar (2003b) during flow boiling of water ($x < 0.15$) and during flow boiling of R-134a ($x = 0.4-0.8$). These correlations also overpredict the experimental data obtained by Yen et al. (2003) for convective boiling of HCFC 123 and FC72 in $d = 190 \mu\text{m}$ tubes in the range of $x = 0.4-0.9$.

Experiments by Lee and Mudawar (2005b) revealed a range of parameters in which heat transfer is controlled by nucleate boiling or annular film evaporation. The micro-channels were formed by cutting 53 of 231 μm wide and 713 μm deep micro-slots into the $25.3 \times 25.3 \text{ mm}^2$ top surface on an oxygen-free copper block. A transparent cover plate formed a top-insulating surface for the micro-channels. Experimental operating conditions spanned the following ranges: inlet quality of $x_{e,\text{in}} = 0.001-0.25$, outlet quality of $x_{e,\text{out}} = 0.49$ to superheat, mass flux of $G = 127-654 \text{ kg}/\text{m}^2 \text{s}$, heat flux of $q = 159-938 \text{ kW}/\text{m}^2$, and inlet pressure of $P_{\text{in}} = 1.44-6.60 \text{ bar}$.

Two-phase heat transfer in micro-channel heat sink was associated with different mechanisms for low, medium, and high-quality flows. Bubble flow and nucleate boiling occur only at low qualities ($x_e < 0.05$) corresponding to very low heat fluxes. High fluxes produce medium-quality ($x_e = 0.05-0.55$) or high-quality ($x_e = 0.55-1.0$) flows depending on the flow rate, where heat transfer is dominated by annular film evaporation. Due to the large differences in heat transfer mechan-

isms between the three quality regions, Lee and Mudawar (2005b) reported that better predictions are possible by dividing the quality range into smaller ranges corresponding to these flow transitions.

Table 6.8 summarizes the new correlations for the three quality regions. The low and high-quality regions are based solely on the Martinelli parameter, while the mid-range includes the effects of Bo and We_L as well. Overall, convection to liquid is important for both the low and mid-quality regions, while convection to vapor becomes important for the high-quality region. For the latter, the low viscosity of R-134a vapor yields vapor Reynolds numbers corresponding to turbulent flow at high-heat flux conditions despite the small hydraulic diameter of the micro-channel. Thus, the single-phase vapor term in the high-quality correlation must allow for both laminar and turbulent vapor flow. The present correlations show that the heat transfer coefficient is proportional to the Martinelli parameter raised to a positive exponent, whereas prior macro-channel correlations employ a negative exponent for the same parameter.

Critical heat flux in flow boiling

Available CHF databases in the literature for flow boiling of water in small-diameter tubes were collected by Zhang et al. (2006). Three correlations by Bowring, Katto and Shah were evaluated with the CHF data for saturated flow boiling, and three correlations by Inasaka and Nariyai, Celata et al. and Hall and Mudawar were evaluated with the CHF data for subcooled flow boiling. The results obtained by Zhang et al. (2006) are presented in Sect. 6.4.3. The collected database included 2,539 points for saturated CHF and 1,298 points for subcooled CHF, covering a wide range of parameters, such as outlet pressures from 0.101 to 19.0 MPa, mass fluxes from 5.33 to 1.34×10^5 kg/m²s, critical heat fluxes from 0.094 to 276 MW/m², hydraulic diameters of channels from 330 to 6.22 mm, length-to-diameter ratios from 1.00 to 975, inlet qualities from -2.35 to 0, and outlet thermal equilibrium qualities from -1.75 to 1.00. A new simple correlation (6.59) was developed by Zhang et al. (2006) for saturated CHF in small-diameter tubes. In contrast to other correlations, this correlation consists only of a single equation and predicts the experimental data with mean deviation of 16.8%. The authors concluded that the correlation may be used to predict CHF of saturated flow boiling in small-diameter tubes. However, results presented by Zhang et al. (2006) consider the macro-scale flow boiling methods adapted to micro-channel data without recognizing any new heat transfer mechanisms. Such an approach cannot explain the disagreement between experimental results discussed above in Chap. 2. In particular, there is significant scatter between results obtained by Wojtan et al. (2006) and Qu and Mudawar (2004). Hence, additional phenomena, channel geometry, surface roughness, instability effects, additives to fluid, and heat transfer mechanisms must have an effect on micro-channel boiling.

The Hall–Mudawar correlation (6.61) seem to be the most reliable tools for CHF prediction in subcooled flow boiling regions.

Table 7.2 Physical properties of saturated water

T [°C]	p (10^{-2}) [kPa]	ρ [kg/m ³]	h [kJ/kg]	c_p [kJ/kg K]	k (10^2) [W/m K]	α (10^8) [m ² /s]	ν (10^6) [m ² /s]	σ (10^4) [N/m]	Pr
0	1.013	999.9	0	4.212	55.1	13.1	1.789	756.4	13.67
10	1.013	999.7	42.04	4.191	57.4	13.7	1.306	741.6	9.52
20	1.013	998.2	83.91	4.183	59.9	14.3	1.006	726.9	7.02
30	1.013	995.7	125.7	4.174	61.8	14.9	0.805	712.2	5.42
40	1.013	992.2	167.5	4.174	63.5	15.3	0.659	696.5	4.31
50	1.013	988.1	209.3	4.174	64.8	15.7	0.556	676.9	3.54
60	1.013	983.1	251.1	4.179	65.9	16.0	0.478	662.2	2.98
70	1.013	977.8	293.0	4.187	66.8	16.3	0.415	643.5	2.55
80	1.013	971.8	355.0	4.195	67.4	16.6	0.365	625.9	2.21
90	1.013	965.3	377.0	4.208	68.0	16.8	0.326	607.2	1.95
100	1.013	958.4	419.1	4.220	68.3	16.9	0.295	588.6	1.75
110	1.43	951.0	461.4	4.233	68.5	17.0	0.272	569.0	1.60
120	1.98	943.1	503.7	4.250	68.6	17.1	0.252	548.4	1.47
130	2.70	934.8	546.4	4.266	68.6	17.2	0.233	528.8	1.36
140	3.61	926.1	589.1	4.287	68.5	17.2	0.217	507.2	1.26
150	4.76	917.0	632.2	4.313	68.4	17.3	0.203	486.6	1.17
160	6.18	907.0	675.4	4.346	68.3	17.3	0.191	466.0	1.10
170	7.92	897.3	719.3	4.380	67.9	17.3	0.181	443.4	1.05
180	10.03	886.9	763.3	4.417	67.4	17.2	0.173	422.8	1.00
190	12.55	876.0	807.8	4.459	67.0	17.1	0.165	400.2	0.96
200	15.55	863.0	852.5	4.505	66.3	17.0	0.158	376.7	0.93
210	19.08	852.8	897.7	4.555	65.5	16.9	0.153	354.1	0.91
220	23.20	840.3	943.7	4.614	64.5	16.6	0.18	331.6	0.89
230	27.98	827.3	990.2	4.681	63.7	16.4	0.145	310.0	0.88
240	33.48	813.6	1037.5	4.756	62.8	16.2	0.141	285.5	0.87
250	39.78	799.0	1085.7	4.844	61.8	15.9	0.137	261.9	0.86
260	46.94	784.0	1135.7	4.949	60.5	15.6	0.135	237.4	0.87
270	55.05	767.9	1185.7	5.070	59.0	15.1	0.133	214.8	0.88
280	64.19	750.7	1236.8	5.230	57.4	14.6	0.131	191.3	0.90
290	74.45	732.3	1290.0	5.485	55.8	13.9	0.129	168.7	0.93
300	85.92	712.5	1344.9	5.736	54.0	13.2	0.128	144.2	0.97
310	98.70	691.1	1402.2	6.071	52.3	12.5	0.128	120.7	1.03
320	112.90	667.1	1462.1	6.574	50.6	11.5	0.128	98.10	1.11
330	128.65	640.2	1526.2	7.244	48.4	10.4	0.127	76.71	1.22
340	146.08	610.1	1594.8	8.165	45.7	9.17	0.127	56.70	1.39
350	165.37	574.4	1671.4	9.504	43.0	7.88	0.126	38.16	1.60
360	186.74	528.0	1761.5	13.984	39.5	5.36	0.126	20.21	2.35
370	210.53	450.5	1892.5	40.321	33.7	1.86	0.126	4.709	6.79

7.3.4 Natural Convection Boiling

Natural convection boiling of water and surfactants at atmospheric pressure in narrow horizontal annular channels was studied experimentally by Hetsroni et al. (2007) in the range of Bond numbers of 0.185–1.52. The channel length was 24 and 36 mm, the gap size was 0.45, 1.2, 2.2 and 3.7 mm. The heat flux was in the range of 20–500 kW/m², the concentration of surfactant solutions was varied from 10 to 600 ppm. Effect of restriction and channel length on boiling curves is presented in Chap. 2. For water boiling at Bond numbers less than unity, the CHF in restricted space is lower than that in unconfined space. This effect increases with increasing the channel length. For water at Bond number of 1.52, boiling can almost be considered as unconfined. The addition of surfactant led to enhancement of heat transfer compared to water boiling in the same gap size; however, this effect decreased with decreasing gap size. Hysteresis was observed for boiling in degraded surfactant solutions. For the same gap size, CHF in surfactant solutions was significantly lower than that in water.

7.3.5 Explosive Boiling

Hetsroni et al. (2003b, 2003, 2005a,b) observed the explosive saturated boiling regime in micro-channels, which exists before the annular flow regime. The test

Table 7.3 Physical properties of R-11

T [°C]	$p(10^{-2})$ [kPa]	ρ' [kg/m ³]	ρ'' [kg/m ³]	h [kJ/kg]	c_p [kJ/kg K]	$k(10^2)$ [W/m K]	$\alpha(10^7)$ [m ² /s]	$\nu(10^6)$ [m ² /s]	$\sigma(10^4)$ [N/m]	Pr
-40	0.05093	1620.7	0.3619	204.06	0.84	0.107	0.783	0.605	264.8	7.72
-30	0.09206	1600.8	0.6285	200.69	0.85	0.104	0.772	0.510	253.0	6.60
-20	0.1576	1579.0	1.037	197.29	0.86	0.101	0.761	0.444	240.3	5.83
-10	0.2573	1554.7	1.633	193.84	0.86	0.098	0.747	0.394	224.6	5.27
0	0.4030	1534.4	2.477	190.34	0.87	0.095	0.733	0.354	212.8	4.83
10	0.6083	1511.5	3.630	186.79	0.88	0.093	0.716	0.324	201.0	4.52
20	0.8891	1487.9	5.165	183.17	0.88	0.090	0.697	0.300	186.3	4.30
30	1.263	1463.7	7.158	179.45	0.89	0.87	0.678	0.277	173.6	4.09
40	1.748	1439.0	9.709	175.60	0.90	0.084	0.658	0.260	160.8	3.95
50	2.366	1413.8	12.900	171.53	0.91	0.081	0.636	0.245	149.1	3.85
60	3.138	1387.9	16.858	167.35	0.92	0.078	0.614	0.232	137.3	3.78
70	4.088	1361.3	21.697	162.87	0.93	0.075	0.591	0.222	123.6	3.76
80	5.240	1333.9	27.579	158.09	0.95	0.073	0.566	0.212	111.8	3.74
100	8.253	1275.8	43.196	147.46	0.98	0.0670	0.539	0.200	89.2	3.72
120	12.393	1211.8	65.660	135.03	1.02	0.061	0.505	0.189	66.7	3.74
140	17.896	1138.3	98.619	120.22	1.07	0.056	0.466	0.183	45.1	3.92

modules had 13, 21 and 26 triangular micro-channels with hydraulic diameters of 220, 130, and 100 μm , respectively. Tests were performed in the range of mass flux 32–200 $\text{kg}/\text{m}^2\text{s}$, heat flux 120–270 kW/m^2 , and vapor quality at the outlet manifold 0.01–0.08. The matter is discussed in Sect. 6.5.1. During quasi-periodic boiling in a certain single micro-channel of a heat sink the pressure drop oscillations were always accompanied by wall temperature oscillations. The period of these oscillations was very short and the oscillation amplitude increased with an increase in heat input. The dependence of the dimensionless time interval between cycles in a given channel on boiling number is shown in Eq. (6.62). The initial liquid film thickness may be calculated using Eq. (6.65). The high-frequency oscillations in individual micro-channels are superimposed and lead to total low frequency (2–5 Hz) pressure drop and temperature oscillations of the whole heat sink. Temporal variations of pressure drop, fluid temperature at the outlet manifold and heater temperature are periodic with the same oscillation frequency. All these fluctuations are in phase. The CHF phenomenon is different from that observed in channels of conventional size. A key difference between micro-channel heat sink and conventional channels is the amplification of instability prior to CHF. The heat transfer coefficient may be calculated with standard deviation of 18% by Eq. (6.66).

7.4 Selected Properties of Liquids Used for Cooling Micro-Devices

The data of physical properties of saturated water are presented in Table 7.2.

Table 7.4 Physical properties of R-12

T [°C]	p (10^{-2}) [kPa]	ρ' [kg/m^3]	ρ'' [kg/m^3]	h [kJ/kg]	c_p [kJ/kg K]	k (10^2) [W/m K]	α (10^7) [m^2/s]	ν (10^6) [m^2/s]	σ (10^4) [N/m]	Pr
–40	0.6423	170.95	1515	4.096	0.8834	0.1000	0.747	0.280	180.44	3.79
–30	1.0052	167.43	1486	6.201	0.8960	0.0954	0.716	0.254	165.73	3.55
–20	1.5102	163.62	1457	9.039	0.9085	0.0907	0.685	0.236	152.98	3.44
–10	2.1927	159.48	1426	12.80	0.9211	0.0861	0.656	0.220	137.29	3.36
0	3.0881	154.95	1394	17.66	0.9337	0.0814	0.625	0.211	124.05	3.38
10	4.2933	150.05	1361	23.80	0.9504	0.0768	0.594	0.204	110.81	3.44
20	5.6731	144.70	1327	31.52	0.9672	0.0721	0.562	0.199	98.06	3.55
30	7.4451	138.75	1292	41.16	0.9839	0.0675	0.531	0.194	85.32	3.66
40	9.5947	132.14	1254	53.12	1.0006	0.0628	0.500	0.191	71.59	3.82
50	12.1463	124.56	1213	68.56	1.0844	0.0582	0.442	0.186	61.19	4.12
60	15.1814	116.90	1167	85.69	1.1179	0.0535	0.410	0.184	42.76	4.49
70	18.7265	108.02	1108	108.81	1.1597	0.0477	0.368	0.183	32.07	4.97
80	22.8393	97.68	1064	138.31	1.2225	0.0419	0.322	0.182	24.12	5.65

Refrigerants R-N (N = 11, 12, ...)

The same data on physical properties of liquid refrigerants R-N (R-11, R-12, R-13, R-21, R-22, R-113) and their vapor are presented in Tables 7.3–7.8. The detailed data on thermophysical properties of different refrigerants (density, enthalpy, heat capacity, viscosity, thermal conductivity and diffusivity) are found in books by Platzer et al. (1990), Andersen (1959), and Danilova et al. (1976).

Many micro-channel blocks have a high thermal conductivity and conjugate effects may become important. In this chapter we considered analytical and experi-

Table 7.5 Physical properties of R-13

T [°C]	p (10^{-2}) [kPa]	ρ' [kg/m ³]	ρ'' [kg/m ³]	h [kJ/kg]	c_p [kJ/kg K]	k (10^2) [W/m K]	α (10^7) [m ² /s]	ν (10^6) [m ² /s]	σ (10^4) [N/m]	Pr
-110	0.161	162.57	1634	1.257	0.816	0.114	0.855	0.408	204.0	4.77
-100	0.333	158.47	1597	2.457	0.854	0.109	0.799	0.340	186.0	4.26
-90	0.628	154.00	1558	4.427	0.879	0.104	0.760	0.298	168.0	3.92
-80	1.098	149.26	1520	7.452	0.908	0.0984	0.712	0.261	151.0	3.67
-70	1.805	144.19	1481	11.848	0.929	0.0933	0.677	0.240	134.0	3.55
-60	2.817	138.62	1439	18.044	0.971	0.0882	0.631	0.221	117.9	3.50
-50	4.204	132.43	1395	26.497	1.009	0.0831	0.590	0.204	101.3	3.46
-40	6.051	125.56	1349	37.850	1.042	0.0780	0.555	0.199	85.5	3.59
-30	8.42	117.98	1300	52.938	1.072	0.0729	0.523	0.194	69.9	3.72
-20	11.43	109.53	1247	72.833	1.105	0.0678	0.493	0.192	54.9	3.90

Table 7.6 Physical properties of R-21

T [°C]	p (10^{-2}) [kPa]	ρ' [kg/m ³]	ρ'' [kg/m ³]	h [kJ/kg]	c_p [kJ/kg K]	k (10^2) [W/m K]	α (10^7) [m ² /s]	ν (10^6) [m ² /s]	σ (10^4) [N/m]	Pr
-40	0.093	1514.1	0.4989	267.1	1.001	0.123	0.814	0.415	277.5	5.10
-30	0.162	1492.7	0.8563	262.1	1.009	0.119	0.795	0.372	261.8	4.68
-20	0.277	1470.9	1.395	256.7	1.017	0.116	0.775	0.337	247.1	4.35
-10	0.454	1448.5	2.180	252.0	1.026	0.113	0.758	0.312	231.4	4.11
0	0.706	1425.6	3.276	246.7	1.034	0.109	0.742	0.288	216.7	3.88
10	1.06	1402.2	4.756	241.7	1.042	0.105	0.725	0.271	202.0	3.74
20	1.53	1378.2	6.708	236.3	1.051	0.102	0.705	0.256	187.3	3.63
30	2.15	1353.8	9.229	230.9	1.059	0.098	0.690	0.244	173.6	3.54
40	2.95	1328.8	12.43	224.4	1.068	0.095	0.672	0.233	159.8	3.47
50	3.96	1302.4	15.87	218.1	1.072	0.091	0.658	0.224	146.1	3.40
60	5.216	1277.4	21.50	211.2	1.080	0.087	0.642	0.216	133.4	3.37
70	6.76	1250.7	27.03	203.8	1.089	0.083	0.622	0.210	119.6	3.38
80	–	1225.4	47.62	196.3	1.097	0.080	0.597	0.205	109.8	3.44

Table 7.7 Physical properties of R-22

T [°C]	p (10^{-2}) [kPa]	ρ' [kg/m ³]	ρ'' [kg/m ³]	h (10^{-3}) [kJ/kg]	c_p [kJ/kg K]	k (10^2) [W/m K]	α (10^7) [m ² /s]	ν (10^6) [m ² /s]	σ (10^4) [N/m]	Pr
-70	2048	1489	1.064	250.58	0.9504	0.1344	0.879	0.434	230.48	3.94
-60	0.3746	1465	1.869	245.05	0.9835	0.1198	0.831	0.323	215.25	3.88
-50	0.6472	1439	3.096	239.48	1.0161	0.1163	0.795	0.275	201.03	3.46
-30	1.6465	1382	7.407	227.55	1.0819	0.1082	0.724	0.232	168.67	3.20
-20	2.4614	1350	10.76	220.94	1.1145	0.1035	0.688	0.218	152.00	3.17
-10	3.5598	1318	15.29	214.36	1.1476	0.1000	0.661	0.210	136.31	3.18
0	5.0013	1285	21.23	206.95	1.1803	0.0954	0.629	0.204	120.13	3.25
10	6.8547	1249	28.90	198.29	1.2129	0.0907	0.599	0.199	103.95	3.32
20	9.1691	1213	38.76	188.41	1.2460	0.0872	0.577	0.197	90.12	3.41
30	12.0228	1176	51.55	177.27	1.2786	0.0826	0.549	0.196	75.90	3.55
40	15.4845	1132	67.57	164.75	1.3117	0.0790	0.532	0.196	60.21	3.67
50	19.6424	1084	88.50	155.33	1.3444	0.0744	0.510	0.196	46.68	3.78
60	24.4378	1032	111.48	149.13	1.3732	0.0709	0.500	0.202	33.69	3.92
70	30.0765	969	146.18	142.00	1.4068	0.0669	0.491	0.208	21.28	4.11
80	36.5979	895	196.35	134.50	1.4403	0.0628	0.487	0.219	11.18	4.41

Table 7.8 Physical properties of R-113

T [°C]	p (10^{-2}) [kPa]	ρ' [kg/m ³]	ρ'' [kg/m ³]	h [kJ/kg]	c_p [kJ/kg K]	k (10^2) [W/m K]	α (10^7) [m ² /s]	ν (10^6) [m ² /s]	σ (10^4) [N/m]	Pr
0	0.148	1626	1.23	160.56	0.9127	0.0766	0.517	0.573	215.25	11.15
10	0.236	1600	1.90	157.97	0.9295	0.0743	0.500	0.506	202.01	10.10
20	0.364	1580	2.85	154.97	0.9462	0.0722	0.483	0.447	192.21	9.23
30	0.541	1560	4.12	152.95	0.9630	0.0702	0.467	0.394	182.40	8.45
40	0.783	1530	5.59	148.84	0.9797	0.0681	0.456	0.359	168.18	7.88
50	1.101	1510	8.00	146.12	0.9965	0.0661	0.439	0.323	158.86	7.35
60	1.512	1480	10.8	145.70	1.0090	0.0640	0.428	0.302	144.16	7.06
70	2.033	1460	14.2	138.88	1.0258	0.0620	0.414	0.278	136.31	6.71
80	2.677	1430	18.5	135.11	1.0425	0.0598	0.403	0.254	124.54	6.30
90	3.472	1400	23.7	130.71	1.0593	0.0578	0.389	0.236	111.79	6.07
100	4.421	1380	30.0	126.11	1.0760	0.0556	0.375	0.218	102.97	5.82

mental correlations for pressure drop and heat transfer, suggested for use in single-phase and two-phase flow in micro-channels, as well as in conventional size channels. It is recommended that such correlations be used in the range of boundary conditions and experimental parameters under which they were obtained.

References

- Ali MI, Sadatomi M, Kawaji M (1993) Two-phase flow in narrow channels between two plates. *Can J Chem Eng* 71:657–666
- Andersen SA (1959) Automatic refrigeration. McLaren, Glasgow
- Armand AA (1946) The resistance during the movement of a two-phase system in horizontal pipes. *Izv Vses Teplotekh Inst* 1:16–23 (AERE-Lib/Trans 828)
- Bergles AE, Rohsenow WW (1964) The determination of forced-convection surface-boiling heat transfer. *Trans ASME J Heat Transfer* 86:365–372
- Celata GP, Cumo M, Marconi V, McPhail SJ, Zummo Z (2005) Micro-tube heat transfer scaling effects: an experimental validation. In: ECI Conference on Heat Transfer and Fluid Flow in Microscale II Ciocco, Castelvechio Pascoili, 25–30 September 2005
- Danilova GN, Filatkin VN, Scherbov MG, Buchko NA (1976) The book of heat and mass transfer problems for food and refrigerating industry. Food Industry, Moscow
- Hetsroni G, Gurevich M, Mosyak A, Rozenblit R (2004) Drag reduction and heat transfer of surfactants flowing in a capillary tube. *Int J Heat Mass Transfer* 47:3797–3809
- Hetsroni G, Mosyak A, Pogrebnyak E, Segal Z (2007) Natural convection boiling of water and surfactants in narrow horizontal channels. *Int J Multiphase Flow* 33:469–483
- Hetsroni G, Mosyak A, Pogrebnyak E, Yarin LP (2005a) Heat transfer in micro-channels: Comparison of experiments with theory and numerical results. *Int J Heat Mass Transfer* 48:5580–5601
- Hetsroni G, Mosyak A, Segal Z, Pogrebnyak E (2005b) Explosive boiling of water in parallel micro-channels. *Int J Multiphase Flow* 31:371–392
- Hetsroni G, Mosyak A, Segal Z, Pogrebnyak E (2003b) Two-phase flow pattern in parallel micro-channels. *Int J Multiphase Flow* 29:344–360
- Hetsroni G, Mosyak A, Segal Z, Pogrebnyak E (2003) Two-phase flow pattern in parallel micro-channels. *Int J Multiphase Flow* 29:344–360
- Hsu YY (1962) On size range of active nucleation cavities on a heating surface. *J Heat Transfer* 84:207–216
- Kandlikar SG (2004) Heat transfer mechanisms during flow boiling in micro-channels. *ASME J Heat Transfer* 126:8–16
- Kandlikar SG, Joshi S, Tian S (2003) Effect of surface roughness on heat transfer and fluid flow characteristics at low Reynolds numbers in small diameter tubes. *Heat Transfer Eng* 24:4–16
- Kawahara A, Chung PM, Kawaji M (2002) Investigation of two-phase flow pattern, void fraction and pressure drop in a micro-channel. *Int J Multiphase Flow* 28:1411–1435
- Kennedy JE, Roach GM, Dowling ME, Abdel-Khalik SI, Ghiaasiaan SM, Jeter SM, Quershi ZH (2000) The onset of flow instability in uniformly heated horizontal micro-channels. *Trans ASME J Heat Transfer* 122:118–125
- Klein D, Hetsroni G, Mosyak A (2005) Heat transfer characteristics of water and APG surfactant solution in micro-channel heat sink. *Int J Multiphase Flow* 31:393–415
- Lee J, Mudawar I (2005a) Two-phase flow in high-heat-flux micro-channel heat sink for refrigeration cooling applications. Part I: pressure drop. *Int J Heat Mass Transfer* 48:928–940
- Lee J, Mudawar I (2005b) Two-phase flow in high-heat-flux micro-channel heat sink for refrigeration cooling applications. Part II: heat transfer characteristics. *Int J Heat Mass Transfer* 48:941–955
- Maranzana G, Perry I, Maillet D (2004) Mini and Micro-channels: Influence of axial conduction in the walls. *Int J Heat Mass Transfer* 47:3993–4004
- Platzer B, Plot A, Maurer G (1990) Thermophysical properties of refrigerants. Springer, Berlin Heidelberg New York
- Qu W, Mudawar I (2003a) Measurement and prediction of pressure drop in two-phase micro-channel heat sinks. *Int J Heat Mass Transfer* 46:2737–2753
- Qu W, Mudawar I (2003b) Flow boiling heat transfer in two-phase micro-channel heat sinks. I. Experimental investigation and assessment of correlation methods. *Int J Heat Mass Transfer* 46:2755–2771

- Qu W, Mudawar W (2004) Measurement and correlation of critical heat flux in two-phase micro-channel heat sinks. *Int J Heat Mass Transfer* 47:2045–2059
- Shah RK, London AL (1978) Laminar flow forced convection in ducts: a source book for compact heat exchanger analytical data. *Advances in Heat Transfer*, suppl 1. Academic, New York
- Steinke ME, Kandlikar SG (2004) An experimental investigation of flow boiling characteristics of water in parallel micro-channels. *Trans ASME J Heat Transfer* 126:518–526
- Tiselj I, Hetsroni G, Mavko B, Mosyak A, Pogrebnyak E, Segal Z (2004) Effect of axial conduction on heat transfer in micro-channels. *Int J Heat Mass Transfer* 47:2551–2565
- Wojtan L, Revellin R, Thome IR (2006) Investigation of saturated critical heat flux in a single, uniformly heated micro-channel. *Exp Thermal Fluid Sci* 30:765–774
- Yen TH, Kasagi N, Suzuki Y (2003) Forced convective boiling heat transfer in micro-tubes at low mass and heat fluxes. *Int J Multiphase Flow* 29:1771–1792
- Zhang W, Hibiki T, Mishima K, Mi Y (2006) Correlation of critical heat flux for flow boiling of water in mini-channels. *Int J Heat Mass Transfer* 49:1058–1072
- Zhao TS, Bi QC (2001) Pressure drop characteristics of gas–liquid two-phase flow in vertical miniature triangular channels. *Int J Heat Mass Transfer* 44:2523–2534

Nomenclature

a	Half length of channel bottom
b	Half length of channel side
d	Diameter
c_p	Heat capacity at constant pressure
C	Concentration
G	mass flux
H	Heat transfer coefficient
k	Thermal conductivity
k_s	Average height of surface roughness
L	Length
n	Exponent (Eq. 7.2)
P	Pressure
q	Heat flux
T	Temperature
x	Mass quality
$D = \frac{\Delta T_{\text{sub,ONB}}}{T_S}$	Parameter
$\text{Nu} = \frac{hd_h}{k}$	Nusselt number
Po	Poiseuille number
$\text{Pr} = \frac{\nu}{\alpha}$	Prandtl number
$\text{Re} = \frac{Ud_h}{\nu}$	Reynolds number

Greek symbols

α	Void fraction
β	Homogeneous (volumetric)
$\Delta T_{\text{sub,ONB}} = T_S - T_{\text{B,ONB}}$	
λ	Friction factor
ρ	Density
$\Pi = \frac{q}{\rho_L U C_{pL} \Delta T_s}$	

Subscripts

B	Bulk
crit	Critical
e	Equilibrium
exp	Experimental
f	Fluid
G	Gas, mass flux
GS	Gas superficial
h	Hydraulic
H1, H2	Thermal boundary condition at constant wall heat flux
in	Inner, inlet
L	Liquid
LS	Liquid superficial
max	Maximum
o	Out
ONB	ONB point
s	Saturation
T	Thermal boundary condition at constant wall pressure
w	Wall, water